Properties of sub-diffraction limited focusing by optical phase conjugation

M. J. Steel[1], Benjy Marks[1] and Adel Rahmani[2]

[1] *MQPhotonics Research Centre, Dept of Physics and Engineering and Centre for Ultrahigh-bandwidth Devices for Optical Systems (CUDOS), Macquarie University, NSW 2109, Australia*

[2] *Dept of Mathematical Sciences, University of Technology, Sydney, NSW 2007, Australia*

msteel@physics.mq.edu.au

http://www.physics.mq.edu.au/research/phottheory

Abstract: Recent work has demonstrated sub-diffraction limited focusing using time-reversal mirrors and sources in scattering media at microwave frequencies. We numerically investigate the possibility of observing analogous effects in the optical domain using small cylindrical scatterers of realistic dielectric materials combined with an enclosing optical phase conjugate mirror in two-dimensional geometries. Such focusing is possible but appears not to significantly exceed the focusing available from an equivalent homogenized material, and is highly sensitive to precise scatterer configuration.

OCIS codes: (290.4210) Multiple scattering ; (350.4238) Nanophotonics and photonic crystals

References and links

1. T. W. Ebbesen, C. Genet, and S. I. Bozhevolnyi, "Surface-plasmon circuitry," Physics Today **61**, 44–50 (2008).
2. W. L. Barnes, A. Dereux, and T. W. Ebbesen, "Surface plasmon subwavelength optics," Nature **424**, 824–830 (2003).
3. R. J. Blaikie, "Nanoscale optical patterning using evanescent fields and surface plasmons," Int. J. Nanosci. **3**, 405–417 (2004).
4. F. De Fornel, *Evanescent waves from Newtonian optics to atomic optics* (Springer, Berlin, 2000).
5. A. Sentenac and P. Chaumet, "Subdiffraction light focusing on a grating substrate," Phys. Rev. Lett. **101**, 13901:1–4 (2008).
6. L. Markley, A. Wong, Y. Wang, and G. Eleftheriades, "Spatially shifted beam approach to subwavelength focusing," Phys. Rev. Lett. **101**, 113901:1–4 (2008).
7. N. Fabre, L. Lalouat, B. Cluzel, X. Melique, D. Lippens, F. De Fornel, and O. Vanbesien, "Optical Near-Field Microscopy of Light Focusing through a Photonic Crystal Flat Lens," Phys. Rev. Lett. **101**, 073901:1–4 (2008).
8. J. Zhu and G. V. Eleftheriades, "Experimental verification of overcoming the diffraction limit with a volumetric Veselago-Pendry transmission-line lens," Phys. Rev. Lett. **101**, 013902:1–4 (2008).
9. I. M. Vellekoop and A. P. Mosk, "Focusing coherent light through opaque strongly scattering media," Opt. Lett. **32**, 2309–2311 (2007).
10. M. Fink, "Time reversed acoustics," Physics Today **50**, 34–40 (1997).
11. P. Blomgren, G. Papanicolaou, and H. Zhao, "Super-resolution in time-reversal acoustics," J. Acoust. Soc. Am. **111**, 230 (2002).
12. D. Liu, G. Kang, L. Li, Y. Chen, S. Vasudevan, W. Joines, Q. Liu, J. Krolik, and L. Carin, "Electromagnetic time-reversal imaging of a target in a cluttered environment," IEEE Trans. Antennas Propag. **53**, 3058–3066 (2005).
13. G. Lerosey, J. De Rosny, A. Tourin, A. Derode, and M. Fink, "Time reversal of wideband microwaves," Appl. Phys. Lett. **88**, 154101:1–3 (2006).

#119185 - $15.00 USD Received 5 Nov 2009; revised 16 Dec 2009; accepted 28 Dec 2009; published 12 Jan 2010

14. G. Lerosey, J. De Rosny, A. Tourin, and M. Fink, "Focusing beyond the diffraction limit with far-field time reversal," Science **315**, 1120–1122 (2007).
15. H. C. Song, W. A. Kuperman, and W. S. Hodgkiss, "Basin-scale time reversal communications," J. Acoust. Soc. Am **125**, 212–217 (2009).
16. B. E. Henty and D. D. Stancil, "Multipath-enabled super-resolution for rf and microwave communication using phase-conjugate arrays," Phys. Rev. Lett. **93**, 243904:1–4 (2004).
17. G. Lerosey, J. De Rosny, A. Tourin, A. Derode, G. Montaldo, and M. Fink, "Time reversal of electromagnetic waves," Phys. Rev. Lett. **92**, 193904:1–3 (2004).
18. E. N. Leith and J. Upatnieks, "Holographic Imagery Through Diffusing Media," J. Opt. Soc. Am. **56**, 523 (1966).
19. S. M. Jensen and R. W. Hellwarth, "Observation of the time-reversed replica of a monochromatic optical wave," Appl. Phys. Lett. **32**, 166–168 (1978).
20. M. Nieto-Vesperinas and E. Wolf, "Phase conjugation and symmetries with wave fields in free space containing evanescent components," J. Opt. Soc. Am. A **2**, 1429–1434 (1985).
21. A. Desfarges, V. Kermene, B. Colombeau, M. Vampouille, and C. Froehly, "Wave-front reconstruction with a Fourier hologram in a phase-conjugating mirror oscillator," Opt. Lett. **20**, 1940–1942 (1995).
22. D. A. B. Miller, "Time reversal of optical pulses by four-wave mixing," Opt. Lett. **5**, 300–302 (1980).
23. S. H. Tseng and C. Yang, "2-D PSTD Simulation of optical phase conjugation for turbidity suppression," Opt. Express **15**, 16005–16016 (2007).
24. Z. Yaqoob, D. Psaltis, M. Feld, and C. Yang, "Optical phase conjugation for turbidity suppression in biological samples," Nature Photonics **2**, 110–115 (2008).
25. R. Carminati, R. Pierrat, J. De Rosny, and M. Fink, "Theory of the time reversal cavity for electromagnetic fields," Opt. Lett. **32**, 3107–3109 (2007).
26. S. Haroche, "Cavity Quantum Electrodynamics," in "Fundamental Systems in Quantum Optics, Les Houches Session LIII," , J. Dalibard, J. M. Raimond, and J. Zinn Justin, eds. (Elsevier Science Publishers, 1992).
27. V. A. Mandelshtam and H. S. Taylor, "Harmonic inversion of time signals," J. Chem. Phys. **107**, 6756–6769, Erratum, ibid. 109 (10), 4128 (1998). (1997).
28. J. De Rosny and M. Fink, "Overcoming the diffraction limit in wave physics using a time-reversal mirror and a novel acoustic sink," Phys. Rev. Lett. **89**, 14301:1–4 (2002).
29. D. E. Aspnes, "Local-field effects and effective-medium theory: A microscopic perspective," Am. J. Phys. **50**, 704–709 (1982).
30. H. C. Van der Hulst, *Light scattering by small particles* (Dover, New York, 1981).

1. Introduction

Focusing electromagnetic radiation below the diffraction limit (focusing to a spot size of less than $\lambda/2$ for wavelength λ) is of increasing importance in optics and drives much of the current interest in nanooptics and plasmonics [1, 2]. Important applications of sub-diffraction limited (SDL) resolution include nanolithography [3] and in-vivo imaging of biological systems. For the former, SDL focusing is required to obtain the finest resolution possible from UV lithography (for which the sources can not get much shorter in wavelength). For the latter, important information is available from resonances in the visible spectrum but UV illumination could be harmful to the subject, preventing the use of shorter imaging wavelengths.

Most approaches to achieving SDL resolution involve coupling to local evanescent fields since propagating waves, while detectable in the far-field, have an upper bound to their allowed wavevectors, and therefore cannot transport high spatial frequency information. Evanescent fields are not limited in transverse wavevector and so in principle allow much higher resolution, but of course the energy in these modes is strongly localized near the scatterer under study. Therefore the key to progress in SDL imaging has been the precise design of structures to excite and tailor evanescent fields. For example, near-field scanning optical microscopy exploits sub-micron diameter fiber tapers, often with metal coatings [4]. Other strategies use carefully designed grating structures and illumination conditions [5–9]. In general, the more accurate the fabrication of near-field coupling structures, the more controlled and effective is the SDL imaging.

A surprising alternative to this strategy has recently emerged from the field of time-reversal focusing [10–13] (a subject which is rather better known in acoustics than electromagnetics). In time-reversal systems, the goal is to focus wave energy onto a small region, with the incom-

#119185 - $15.00 USD Received 5 Nov 2009; revised 16 Dec 2009; accepted 28 Dec 2009; published 12 Jan 2010

ing waves passing through an intervening highly-disordered multiple-scattering medium, *the detailed structure of which is unknown*. For elastic waves and microwaves, this can be accomplished as illustrated in Fig. 1. In Stage 1 at left, a radiating source (blue) emits waves which are scattered by random objects (black) surrounding the source. The outgoing waves are detected by an array of transducers in the far-field (green) enclosing the target, so that the set of voltages recorded by the transducers effectively contains detailed information about the intervening scattering medium. In Stage 2, the source is switched off and the detected signal at each transducer is reversed in time, amplified and used to excite a new wave (right part of Fig. 1). Provided the medium is reciprocal (lossless and non-magnetic) the time-reversed wave focuses back to the target as the initial phase evolution is undone. The transducer array is thus a "time reversal mirror" (TRM). Note the TRM need not completely enclose the region under study: in some cases, the TRM array is localized but the whole system is surrounded by highly reflecting walls [14]. In other demonstrations however, the TRM has a genuinely finite aperture, and some wide-angle information is lost. Such schemes have been demonstrated in laboratory [10] and marine acoustics [15] and in microwave systems [16, 17], and have been shown to achieve diffraction-limited focusing. In the optical domain, we cannot of course obtain a direct phase-sensitive record of the received electric field, so a literal TRM is impossible. However, the concept of "optical phase conjugation", for example through four wave mixing, has long been used to similar effect [18–21]. For harmonic waves, which is the case considered in this work, optical phase conjugation and time reversal are equivalent [22]. Phase conjugate mirrors have recently been used to produce significant improvement in imaging through highly-scattering biological materials [23, 24], though not beyond the diffraction limit.

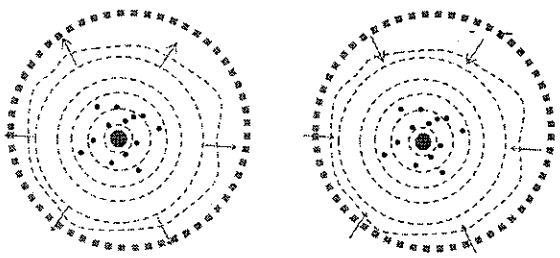

Fig. 1. Schematic of time reversal or phase-conjugate focusing in a disordered scattering medium. In Stage 1 (left), a dipole source emits waves which are multiply scattered before being detected in the far field. In Stage 2 (right), a TRM (green squares) or a phase-conjugate mirror emits a conjugate wave which focuses in the vicinity of the original source.

1.1. Sub-diffraction limited focusing with TRM

Now consider the quality of the time-reversed focus spot, assuming a point source as the origin of the outgoing waves in Stage 1. Since high spatial frequency evanescent components of the radiated field die out close to the source, they can never reach the far-field TRM and so can not be reconstructed at the source in the return stage. We may thus expect that the focus spot diameter D produced by a TRM system is limited to the diffraction limit $D \approx \lambda/2$. (Indeed, even if we admit that in a noiseless system the evanescent waves technically do reach the TRM, the time reversed configuration does not typically include a sink—the time-reversed equivalent of the original source. This absence also prevents reconstruction of the original field to better than

#119185 - $15.00 USD Received 5 Nov 2009; revised 16 Dec 2009; accepted 28 Dec 2009; published 12 Jan 2010

the diffraction limit [28]. We return to this point in more detail in Section 3.) Nevertheless, in an elegant microwave experiment in 2007, Lerosey et al [14] showed that a TRM may produce focusing *below* the diffraction limit, if the source is surrounded by a random array of strong scatterers in the near field region. In the experiment, a set of coaxial antennae operating at $\lambda = 0.122$ m were surrounded by an irregular comb of numerous copper wire scatterers and placed inside a closed box of order 1 m in size containing a small TRM. The authors were able to distinguish between the antennae when separated by only $\lambda/30$, far below the diffraction limit. Lerosey et al interpret this result in terms of the evanescent waves being scattered by the wires into propagating waves which reach the far-field TRM. They thus contribute to the incoming time-reversed wave, and in the near field are re-scattered back into the evanescent components required to reconstruct a sharp focus.

It has subsequently been shown [25] that for a perfect TRM that encloses the domain, the time-reversed electric field $\mathbf{E}^{\text{TRM}}(\mathbf{r})$ can be expressed in terms of the Green function of the system for a souree at $\mathbf{r}_0$:

$$\mathbf{E}^{\text{TRM}}(\mathbf{r}) \propto \text{Im}[\mathbf{G}(\mathbf{r},\mathbf{r}_0)]. \tag{1}$$

In the time harmonic regime, the time-reversed field is thus a standing wave (due to the interference of incoming and outgoing waves,) and its value at the source is proportional to the local density of electromagnetic states (LDOS). Since the LDOS is proportional to the emission rate of the dipole [26] (in the weak-coupling regime relevant here,) this result implies that *the focusing is improved by arrangements of scatterers that promote emission from the source.*

1.2. Objectives—TRM focusing in the optical domain

The experiment of Ref. [14] is an impressive demonstration in the microwave domain, but it is in the optical that new strategies for SDL resolution are most in demand. Thus one wonders to what degree similar focusing can be achieved for optical waves. This question is the subject of the present work. A shift to the optical domain introduces a number of changes. Firstly, as absolute detection of optical phase is impossible, a literal TRM is also impossible. Here we concentrate on time harmonic waves, so that the TRM becomes a phase conjugate mirror (PCM)—that is, a material that reflects an incoming wave with a reversed phase profile, represented by taking the complex conjugate of the incoming electric field. The implementation of the PCM will not concern us here, though it might be a strongly pumped Kerr or photorefractive medium. Secondly, while for microwaves, copper wires are ideal conductors (and strong scatterers for $\mathbf{E}$ polarized along the wires), metals are lossy in the optical domain and dissipation breaks the time reversal symmetry. Therefore we have studied predominantly dielectric scatterers, with physical refractive indices limited to $n \lesssim 6$.

In this paper, we consider a range of two-dimensional (2D) scattering geometries using numerical simulation and explore the different focusing regimes. After describing our numerical procedure in Sec. 2, in Sec. 3 we illustrate the basic focusing mechanism and show the impact of an incomplete PCM. In Sec. 4, we establish that there are two distinct focusing regimes—a *homogenization regime* and a *scattering regime*—and that the behavior is strongly polarization dependent. In Sec. 5, we consider the role of fluctuations in the mirror and scatterer locations, and metallic components.

2. Method of calculation

We have performed a large range of simulations using two-dimensional (2D) Finite-Difference Time-Domain (FDTD) simulation. A harmonic dipole point source is located inside a cloud of randomly arranged identical cylindrical sub-wavelength scatterers. The individual scatterers are characterized by their radius a_s and refractive index n_s. The background index has the value

#119185 - $15.00 USD Received 5 Nov 2009; revised 16 Dec 2009; accepted 28 Dec 2009; published 12 Jan 2010

$n_b = 1$, unless otherwise stated. Although it might be challenging to implement a completely enclosing optical phase conjugate mirror, it is in principle possible. We make this assumption for most of our examples, for the sake of simplicity and computational efficiency (explained below). The time-reversed field is calculated in two ways. In the "first principles" approach, the complex amplitude of the field radiated by the Stage 1 dipole source is determined at a ring of equally-spaced field monitors located in the far-field region, by applying the filter diagonalization method [27] to the time series of the electric field recorded at each monitor. (Note that as evanescent waves decay very rapidly with distance from the source, placing the detectors a distance of approximately λ–2λ from the source is sufficient to capture the far-field behavior.) The monitors are separated by $\lambda/2$ or less, so that the propagating field is fully resolved. For Stage 2, the monitors are replaced by harmonic dipole sources, emitting with a relative temporal phase which is the conjugate of the measured phase distribution of the initial outgoing wave. The simulation is run until a steady state field is obtained, which represents the time-reversed wave.

The second approach makes use of Eq. (1). The Stage 1 field generated by the dipole source is by construction the time-dependent Green function, and so the time-reversed field can be found directly from Eq. (1). This method is substantially faster, because only the near field region containing the scatterers needs to be included in the Stage 1 simulation domain size, and because Stage 2 is avoided completely. However, Eq. (1) only holds for an ideal closed TRM [25]. While less efficient, the "first-principles" method allows study of a range of non-ideal situations including an incomplete or imperfect TRM, or an arrangement of scatterers which differs on the return path.

2.1. *Numerical parameters*

As a 2D isotropic system, our problem is separable, and for propagation in the $x-y$ plane, we consider both E_z (**E** out of plane) and H_z (**E** in plane) polarization. Thus the true physical system being modeled is a cluster of dielectric *cylinders* with a harmonic *line* source. Throughout we use dimensionless units where length is scaled by the wavelength λ. The spatial grid in the FDTD simulations was either $\Delta x = 0.004$ or $\Delta x = 0.002$, sufficient to resolve the fields in the smallest scatterers. With this resolution, the reconstructed field was found to be essentially independent of the precise grid size. We use scatterers with refractive indices, $n_s = 3$, 4 or 6. (The last two values are somewhat high for the optical regime, but help to illuminate the physics in certain cases that would otherwise show very weak scattering.) The scatterer radius varies from $a_s = 0.006$ to $a_s = 0.018$, and the typical scatterer spacing is of order $\delta x \approx 0.01$.

3. Demonstration of macroscopic focusing behavior

Before investigating the potential for SDL focusing, we demonstrate the basic properties of time-reversal focusing with the scatterers lying *beyond* the near-field region. Figure 2 illustrates different aspects of the field behavior for two TRM configurations. The first four plots show the radiated and reconstructed field for a E_z-polarized dipole located at $\mathbf{r}_0 = (1,0)$ surrounded by a complete TRM. Fifteen dielectric scatterers (black circles in Fig. 2(a)) are placed randomly in the far-field region ($r \gtrsim \lambda$). For this case only, the FDTD grid resolution is $\Delta x = 0.01$. The real part of the time-reversed field $\mathrm{Re}[E_z^{\mathrm{TRM}}(\mathbf{r})]$ in Fig. 2(b) is an almost perfect reconstruction of the emitted field in Fig. 2(a), with the diffraction-limited spot reconstructed at $\mathbf{r} = (1,0)$. Figure 2(c) shows the imaginary part of the time-reversed field $\mathrm{Im}[E_z^{\mathrm{TRM}}(\mathbf{r})]$. Inside the TRM, the imaginary part almost exactly vanishes so that the field is purely real and of standing wave character, consistent with Eq. (1). The standing wave arises because there is no optical sink at the original source point, and the converging waves become diverging waves as they pass through the source point, producing interference [28]. Outside the TRM, there are only outgoing

#119185 - $15.00 USD Received 5 Nov 2009; revised 16 Dec 2009; accepted 28 Dec 2009; published 12 Jan 2010

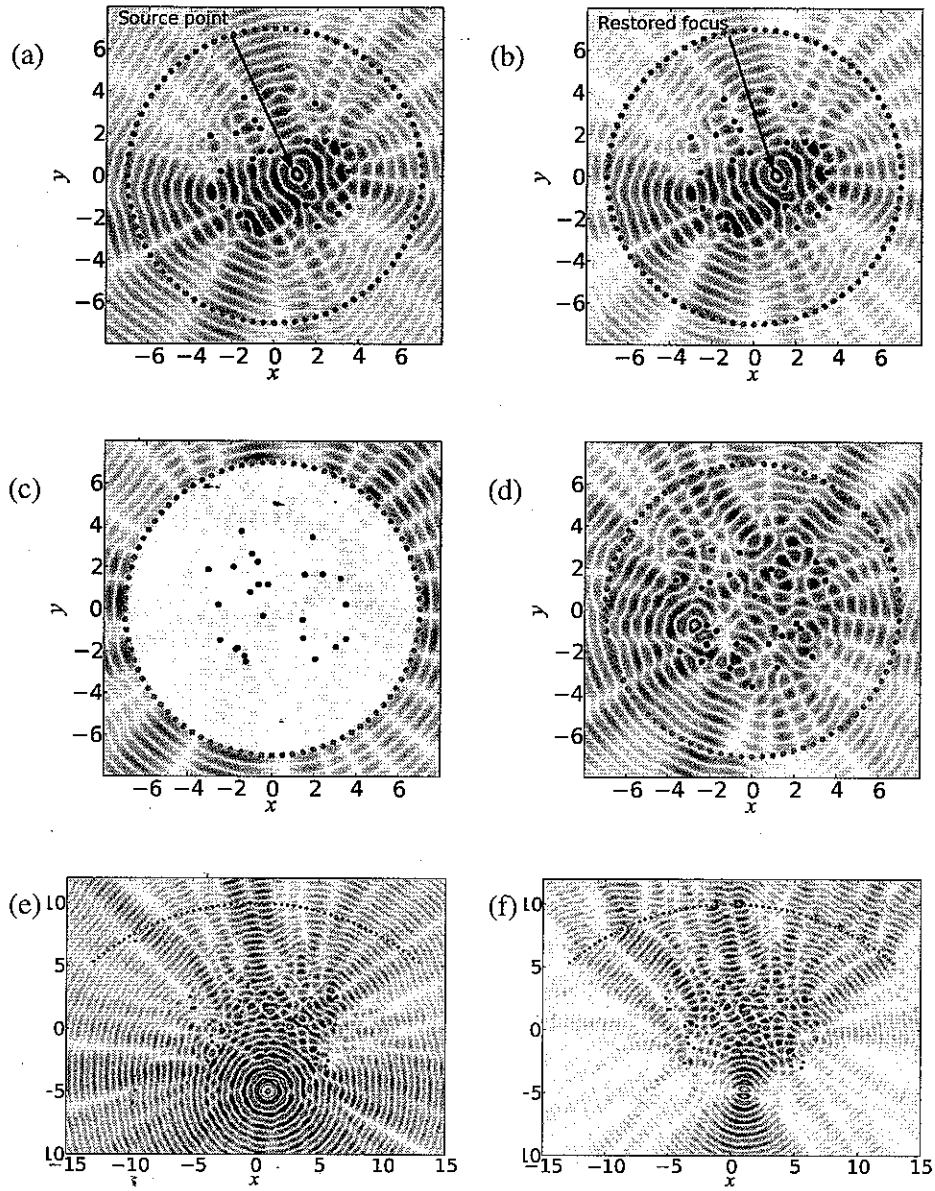

Fig. 2. Illustration of diffraction-limited time-reversal focusing for E_z polarization. The green squares indicate positions at which the field is measured and its conjugate emitted, and are separated by $\lambda/2$. There are $N = 15$ scatterers with the parameters $a_s = 0.15$, $n_s = 2$. (a) Forward field $\mathrm{Re}[E_z(\mathbf{r})]$ radiated by a dipole source at $\mathbf{r} = (1,0)$. (b) Time-reversed field $\mathrm{Re}[E_z^{\mathrm{TRM}}(\mathbf{r})]$ for (a) calculated by the first principles method. (c) Imaginary part of the time-reversed field $\mathrm{Im}[E_z^{\mathrm{TRM}}(\mathbf{r})]$ confirming standing-wave character inside the TRM and propagating-wave character outside. (d) Time-reversed field $\mathrm{Re}[E_z^{\mathrm{TRM}}(\mathbf{r})]$ for (a) with the scatterers repositioned. (e) Forward field $\mathrm{Re}[E_z(\mathbf{r})]$ radiated by a dipole source at $\mathbf{r} = (1,-5)$ with an arc-shaped TRM. (f) Time-reversed field $\mathrm{Re}[E_z^{\mathrm{TRM}}(\mathbf{r})]$ for (e).

#119185 - $15.00 USD Received 5 Nov 2009; revised 16 Dec 2009; accepted 28 Dec 2009; published 12 Jan 2010

waves and so both the real and imaginary parts of the field have the same magnitude (compare the fields outside the TRM in Figs. 2(b) and 2(c)). To illustrate the importance of the conjugate phase information in reconstructing the focus, Fig. 2(d) shows $\mathrm{Re}[E_z^{\mathrm{TRM}}(\mathbf{r})]$, for a situation in which the scatterers are rearranged before the time-reversal stage. The focus at the source point is completely lost. Figures 2(e) (forward field) and 2(f) (time-reversed field) show that the focus reconstruction can still be quite successful for an incomplete mirror (in this case an 80° arc).

4. Response to scatterers in the near-field

We now turn to the core topic of the paper—the nature of time-reversal focusing when the scatterers are much smaller than a wavelength and are located in the near-field region of the source. From a large set of simulations across a significant parameter space we have found two qualitatively different regimes which we characterize as the *homogenization* and *scattering* regimes. We examine the behavior for both E_z and H_z polarization. For efficiency, we have used the Green function method of calculation and show the field structures only in the vicinity of the scatterers. An ideal TRM or phase conjugate mirror may be imagined to surround the simulation domain at a distance of a few wavelengths.

4.1. *Scattering regimes for E_z polarization*

In a uniform material of refractive index n, the dipole source generates cylindrical waves and the time-reversed wave is expected to have the form $E_z(r) \propto J_0(2\pi nr/\lambda)$, where $J_0(x)$ is the zeroth-order Bessel function of the first kind. Thus a reasonable definition of the spot size D of the focus is the diameter of the zero-intensity ring,

$$D_{\mathrm{uni}}(n) = 2r_1 \frac{\lambda}{2\pi n} \approx \frac{0.765\lambda}{n}, \qquad (2)$$

where $r_1 \approx 2.4046$ is the first zero of $J_0(r)$. We now consider the spot size when the source is embedded in a cloud of scatterers. The circular scatterers, with radius a_s and index contrast Δn are arranged on a square grid with mean spacing s, but with each scatterer having a random displacement of $\delta\mathbf{r}_j = s(\delta x_j, \delta y_j)$ where δx_j and δy_j are uniform random variables in the range $[-\tau/2, \tau/2]$. The source is placed off-center but well within the cloud. Within this parameter space we have performed hundreds of simulations. Note that in some cases, several of the scatterers overlap. In the index generation process for our simulations, these scatterers are simply merged into a single irregular shape of the same index. In calculating averaged refractive indices below, we account for these merged cases.

For small, densely spaced scatterers ($a_s \lesssim \lambda/100$), we always find that the behavior is largely independent of the particular random instance of scatterer locations. The field profile of the time-reversed wave remains similar to a cylindrical wave, and the relation (2) for the diameter $D_{\mathrm{uni}}(n)$ holds very well with the index n replaced by the effective refractive index $\bar{n}_{E_z} = \sqrt{fn_s^2 + (1-f)n_b^2}$, where f is the fraction of the scattering region actually occupied by scatterers. This is the standard long-wavelength homogenization of a two-component composite for E_z polarization [29], which is appropriate for the relatively dilute and uncorrelated arrangement of scatterers we are considering. Figure 3(a) shows a typical focus spot in this regime with $n_s = 4, a_s = 0.008$. Figure 3(b) shows the dependence of D on the homogenized index $\bar{n}_{E_z}$ for a range of scatterer sizes and densities, with Eq. (2) indicated by the blue line. The results for five random instances are shown for each set of parameters, and they clearly track Eq. (2) closely. At larger values of $\bar{n}_{E_z}$, the measured diameter D begins to depart from the homogenization curve. In this regime, the cloud of scatterers collectively starts to act as a weak cavity and the field in the focus region is distorted, somewhat resembling cavity modes, rather than circles. To

#119185 - $15.00 USD Received 5 Nov 2009; revised 16 Dec 2009; accepted 28 Dec 2009; published 12 Jan 2010

accommodate this, the measured values of D are found by calculating the area A bounded by the first zero of the focus spot (the white bands in the insets to Fig. 3) and taking $D = \sqrt{4A/\pi}$. Overall however, the cloud of scatterers behaves as if it were a uniform medium of index $\bar{n}_{E_z}$, with the spot size and position depending very weakly on the precise position and size of the scatterers. We term this the *homogenization* regime.

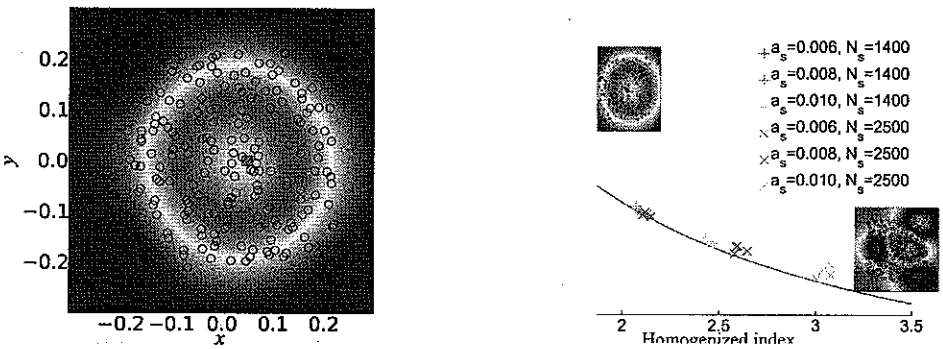

(a) (b)

Fig. 3. Homogenization domain of focusing for E_z polarization. (a) Focus spot region of time-reversed field for a case with 225 scattters having parameters $n_s = 4, a_s = 0.008, s = 0.027, \tau = 0.5$, (corresponding to $\bar{n}_{E_z} = 2.10$). The source is at $\mathbf{r} = (0.05, 0.0)$, indicated by the green box. (b) Measured spot diameters (crosses) and $D_{\text{uni}}(\bar{n}_{E_z})$ (solid) as a function of effective index $\bar{n}_{E_z}$, for an approximate density of N_s scatterers per square wavelength. Insets show focus spots for a case strongly in the homogenization regime (top-left) and a case beginning to show internal structure (lower-right).

We find quite different results for somewhat larger, less dense scatterers. Figure 4(a) shows the time-reversed field configuration for a particular random instance for the parameters: 200 scatterers with $n_s = 5, a_s = 0.014, s = 0.07, \tau = 0.75$, corresponding to a homogenized index of $\bar{n}_{E_z} = 3.33$ and thus a nominal spot diameter of $D_{\text{uni}}(n) = 0.230$. A blow-up of the central region is shown in Fig. 5(a). In this case, the measured focus spot (again defined as the region bounded by the first zero line (white) around the source point) has an effective diameter $D = 0.256$. This is actually slightly larger than D_{uni}, but is of course well below the vacuum spot size of 0.765. However, for this instance, the focus spot only samples approximately 19 scatterers. Calculating the homogenized index just within the spot gives local values $\bar{n}^{\text{loc}}_{E_z} = 2.64$ and $D^{\text{loc}}_{\text{uni}} = 0.290$, so that the actual spot size D is around 12% smaller than might be expected. This is certainly not a dramatic improvement in focusing beyond the homogenization level but shows that improvements are possible. Note that as expected, the fine structure in this plot is entirely in the scattering region—the waves reaching the nominal time reversal mirror in Fig. 4(a) have only low resolution features. A different random instance with the same parameters shown in Figs. 4(b) and 5(b) performs somewhat better, with a measured spot size $D = 0.217$ which is less than the nominal homogenized diameter D_{uni}.

Whereas the behavior in the homogenization regime is essentially independent of the precise location of scatterers and source, the focusing effects in this regime are much more sensitive to the distribution of scatterers and the location of the source. While the cases in Figure 5(a,b) show good focusing, for certain random instances such as in Figs. 5(c) and 5(d) (again with the same parameters) no strong focus spot is obtained, and for Fig. 5(d), the focusing is considerably worse than in the homogenization regime. From the many random instances we have examined, this behavior with no sharp focus is in fact the more common result. The time-reversed

#119185 - $15.00 USD Received 5 Nov 2009; revised 16 Dec 2009; accepted 28 Dec 2009; published 12 Jan 2010

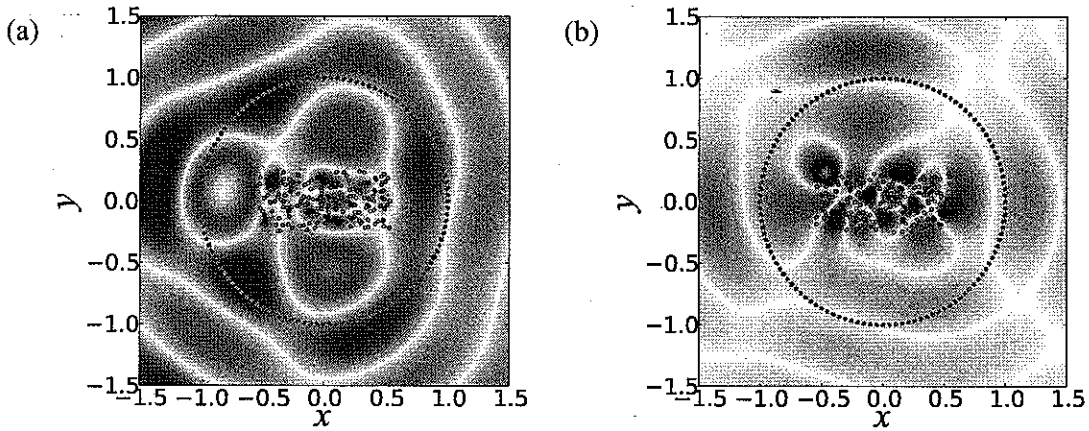

Fig. 4. Scattering domain of focusing for E_z polarization with source at $\mathbf{r}_s = (0.05, 0)$ (green square). (a) Example with 200 scatterers of $n_s = 6, a_s = 0.014, s = 0.0426, \tau = 0.75$. (b) Different random arrangement with same parameters as (a).

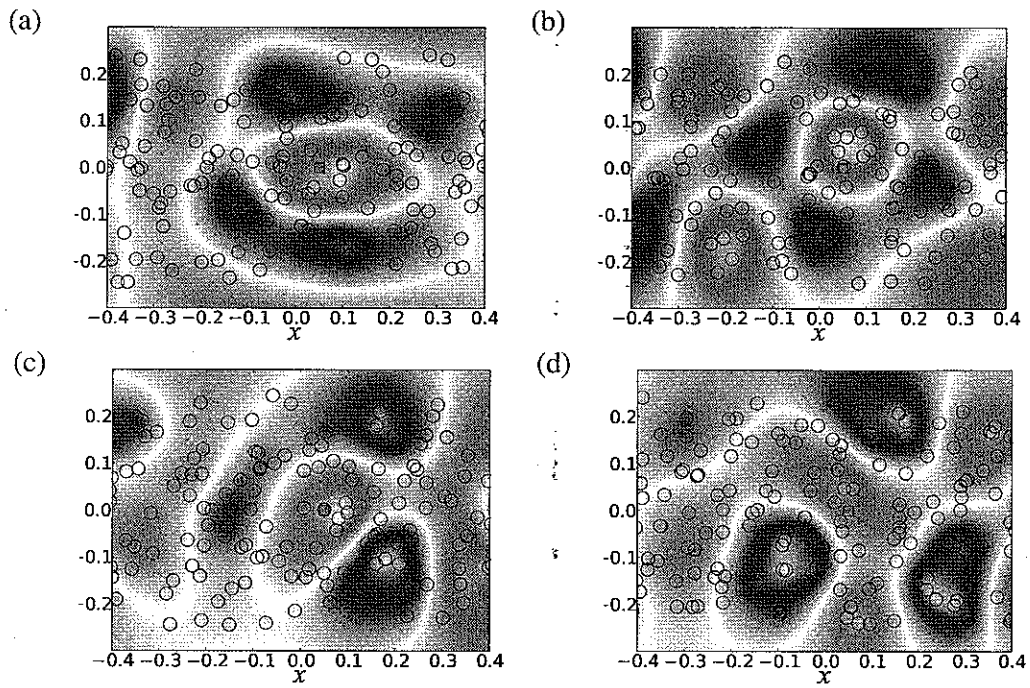

Fig. 5. Close up of scattering region of focusing for E_z polarization. (a) Magnification of central region of Fig. 4(a). (b) Central region for Fig. 4(b). (c) and (d) Central region for two other cases with same parameters but poor hot-spot behavior.

#119185 - $15.00 USD Received 5 Nov 2009; revised 16 Dec 2009; accepted 28 Dec 2009; published 12 Jan 2010

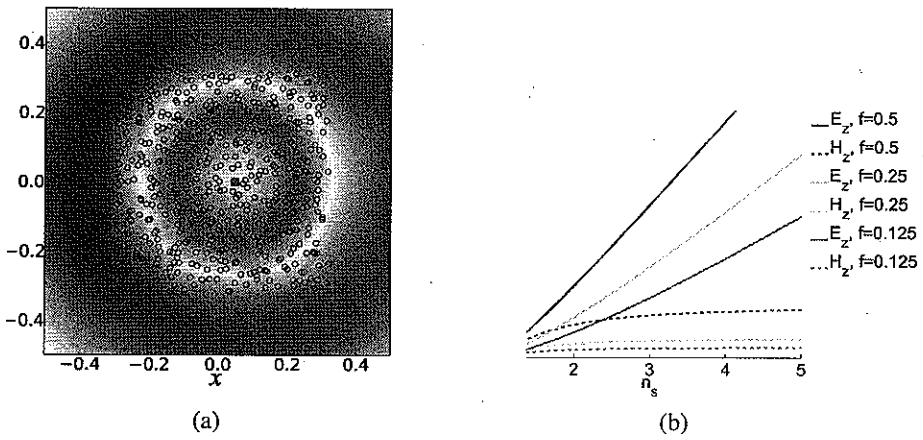

Fig. 6. (a) Re$[H_z]$ component of time-reversed field for H_z polarization, for parameters of Fig. 3(a). (Note change in scale of x and y axes.) (b) Effective indices $\bar{n}_{E_z}$ and $\bar{n}_{H_z}$ as a function of fill fraction f and scatterer index n_s.

field thus displays a "hot-spot" behavior, where the source and scatterers must be fortuitously arranged to attain good focusing. It is interesting that a similar sensitivity to antenna location was observed in the microwave experiments by Lerosey et al (see online material for Ref. [14]). The strong sub-wavelength focusing they observed was only obtained after careful adjustment of the source and surrounding wires, though the degree of optimized focusing obtained was much stronger, due to very strong scattering by metal wires.

4.2. *Scattering regimes for H_z polarization*

We repeated these calculations for a source with H_z polarization. In this case, the Green function becomes a 2×2 Green tensor $G_{ij}(\mathbf{r}, \mathbf{r}')$ and the time reversal mirror is implemented with detectors and dipole sources for both components of the in-plane electric field. In general, we find the focusing properties are much weaker for H_z polarization. Figure 6(a) shows H_z focusing in the homogenization regime for a configuration with the same scattering parameters as in Fig. 3(a), but a somewhat larger cloud (in order to contain the focus spot). We see H_z case produces a considerably larger focus spot, with here $D = 0.56$, as compared to $D = 0.37$ for the E_z case. Similarly, for parameters which exhibit hot spot behavior in the E_z case, we see relatively poor focusing for H_z polarization with no sub-diffraction limited behavior. This contrast in behavior with polarization increases with the index contrast.

We can interpret the weaker focusing for H_z polarization in two ways. The appropriate definition of the homogenized index is not as well defined in the H_z case, as it depends on the local orientation of the electric field at scattering interfaces [29]. Assuming fully perpendicular fields, we can find $\bar{n}_{H_z} = 1/\sqrt{f/\varepsilon_s + (1-f)/\varepsilon_b}$, yielding a mean value considerably lower than $\bar{n}_{E_z}$. Indeed, $\bar{n}_{H_z}$ has an upper bound $\sqrt{\varepsilon_b/(1-f)}$ (see comparison of $\bar{n}_{E_z}$ and $\bar{n}_{H_z}$ in Fig. 6(b)). For arbitrary polarization, the correct homogenized value will lie between $\bar{n}_{H_z}$ and $\bar{n}_{E_z}$, but will certainly be lower than $\bar{n}_{E_z}$. The difference in the two effective indices explains the observation that the difference in focusing behavior between the polarizations increases with index contrast. For another interpretation that also applies in the scattering regime, we can consider the scattering cross section σ (equal to the extinction coefficient in the case of lossless materials) of a

#119185 - $15.00 USD Received 5 Nov 2009; revised 16 Dec 2009; accepted 28 Dec 2009; published 12 Jan 2010

single cylinder [30]. In the limit of small cylinder diameter, the ratio of the cross sections is

$$R_\sigma = \sigma_{E_z}/\sigma_{H_z} = (n^2+1)^2/2, \tag{3}$$

which gives $R_\sigma = 50$, for a scatterer index as low as $n = 3$. The much poorer hot-spot behavior for H_z polarization is thus easy to understand. In the Lerosey experiment, the dipole antenna is aligned with long wire scatterers, so that the field can be regarded as predominantly E_z in nature and the appearance of strong hot-spot scattering is understandable.

5. Other effects

5.1. *Sensitivity to randomness*

Since to achieve SDL focusing by time reversal, one reconstructs the near field entirely from far-field information, we might expect considerable sensitivity to imperfections in the phase conjugate/time-reversal mirror. We modeled this by adding phase noise to the antennae. Each dipole source now radiates with the amplitude $A_j = A_j^0 e^{i\eta_j}$ where A_j^0 is the dipole amplitude for a perfect mirror and η_j is a uniform random variable in the range $[-\eta_m/2, \eta_m/2]$. With an imperfect mirror, Eq. (1) is no longer applicable, so we calculate TR fields by the direct method. As the time-reversed field is no longer purely real, we plot the modulus $|E_z|$. For the scatterer configuration of Fig. 4, Figs. 7 (a)-(d) show the reconstructed field for $\eta_m = 0, 0.75\pi, 1.5\pi$ and 2π (complete randomization of the incoming phase). Surprisingly perhaps, for $\eta_m = 0.75\pi$ the focused field is hardly degraded at all, and even at $\eta_m = 1.5\pi$ the original focus spot is still visible. For complete randomization, the original spot does disappear as expected. Similar robustness to phase errors has been observed in recent experiments on phase conjugate imaging through turbid media [24].

We have also investigated the sensitivity to changes in scatterer location on the return path. Such changes might be associated with imaging of living specimens, or systems using holographic recording where the field reconstruction is performed later or on a different but nominally identical structure. Again starting with the example from Fig. 4a, we shift the location of each scatterer by a random offset $\Delta \mathbf{r}_j = (\rho_j^x, \rho_j^y)$, where ρ^x, ρ^y are uniform random variables in the range $s[-\rho_m, \rho_m]$, with s the mean scatterer spacing. Figures 7(e) and (f) show the reconstructed field for $\rho_m = 0.25$ and $\rho_m = 1$. The original focus spot partially survives with $\rho_m = 0.25$ but is lost for $\rho_m = 1$. However, a new hot spot, even smaller than the original one, has appeared to the lower-right of the original source point. This illustrates that accurate time-reversal is not required in order for hot spots to appear in the final field—they are as much a product of quasi-resonances associated with fluctuations in the scatterer density. However, accurate time-reversal *is* needed to ensure that a hot spot *associated with the original radiating source* can be recovered with the incoming field. It should be obvious that in the homogenized regime represented by Fig. 3a, random rearrangement of the scatterers has essentially no effect on the focusing behavior, as is confirmed by simulations.

5.2. *Ideal metallic scatterers*

With the current widespread interest in near-field enhancement by nano-metallic structures, it is natural to examine the behavior of time-reversal focusing with metal scatterers. We performed a number of simulations with similar parameters to those above but using nominally perfect metal scatterers of $\varepsilon = -1 + 10^{-10}i$. (Note that in the visible, metals exhibit strong dissipation so our calculations do not apply there, but the introduction of loss destroys time-reversal symmetry and strong focusing would be impossible anyhow. The results should however be relevant in the mid-infrared). Surprisingly perhaps, for the 2D geometry considered in this paper, the time-reversed focusing fails completely for interesting reasons.

#119185 - $15.00 USD Received 5 Nov 2009; revised 16 Dec 2009; accepted 28 Dec 2009; published 12 Jan 2010

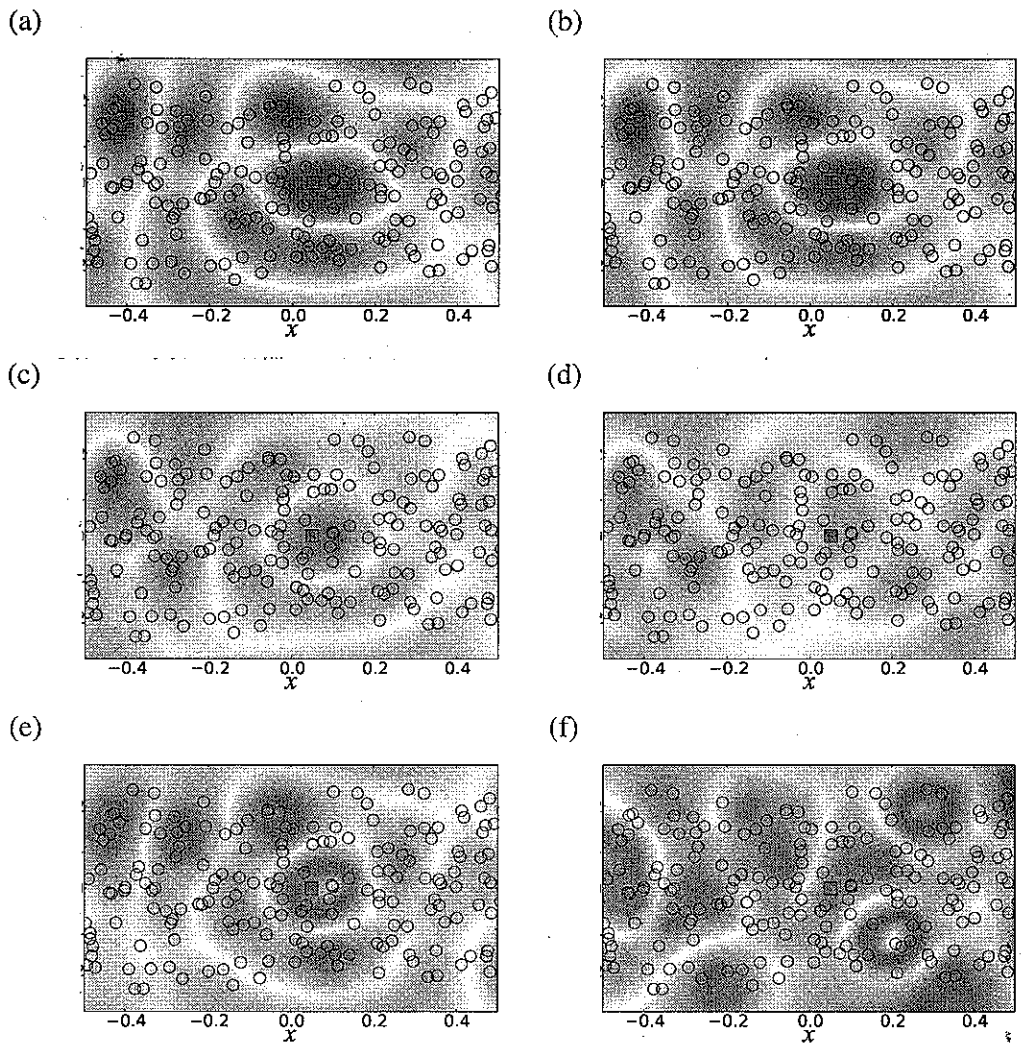

Fig. 7. Stage 2 focused field $|E_z|$ for the scatterer configuration in Fig. 4(a) with phase noise (a) $\eta_m = 0$, (b) $\eta_m = 0.75\pi$ (c) $\eta_m = 1.5\pi$ (d) $\eta_m = 2.0\pi$; and position noise (e) $\rho_m = a/8$, (f) $\rho_m = a$. The green square indicates the location of the original source.

#119185 - $15.00 USD Received 5 Nov 2009; revised 16 Dec 2009; accepted 28 Dec 2009; published 12 Jan 2010

Figure 8(a) shows a snapshot of the electric field produced by an antenna in a representative cluster of metal scatterers. The perfect metal scatterers expel the field and lead to a pattern that is strongly localized with $D \approx 0.06$. However, the time-reversed field predicted by Eq. (1) and illustrated in Fig. 8(b) is completely different and shows that the incoming field from the TRM is almost completely expelled with virtually no energy reaching the interior of the scattering region. This behavior is explained as follows. Recall that for a classical dipole in a closed metallic cavity at a frequency below any resonant cavity modes, on average no energy is coupled into radiation. Instead energy oscillates between the cavity field and the dipole at the driving frequency. For small clusters of metallic scatterers, we invariably find that the scattering is sufficiently strong that the source dipole is effectively contained in an almost perfect cavity, and there is continual exchange of energy between the dipole and a local standing mode field. It is this standing mode that is visible in Fig. 8(a). Only a small fraction of the energy in a single optical cycle escapes beyond the scattering region (for this example, approximately 0.0005 of the peak standing wave energy in each cycle), so that the near field region and the region beyond the scatterers are almost completely decoupled. By the same argument, the incoming field from the TRM couples very weakly to the interior and no significant energy is found inside the scattering region, let alone a strong focus spot. These observations are consistent with Eq. (1). Due to the decoupling from the exterior region, the real part of the Green function near the antennas is three orders of magnitude stronger than the imaginary part in the example shown. Thus the refocused field predicted by Eq. (1) is extremely weak. In fact in the scattering region, $\mathrm{Im}[\mathbf{G}(\mathbf{r},\mathbf{r}_0)]$ will contain features below the diffraction limit, and since the regions are not perfectly decoupled in principle it would in principle be possible to excite local field structures near the original source from the incoming reversed wave. However, as the vast majority of the incoming energy would be reflected by the scatterers this would require enormous gain on the TRM and is quite impractical.

We note that in a 3D geometry, it is easy for the light to escape at glancing incidences and refocusing should be much more feasible.

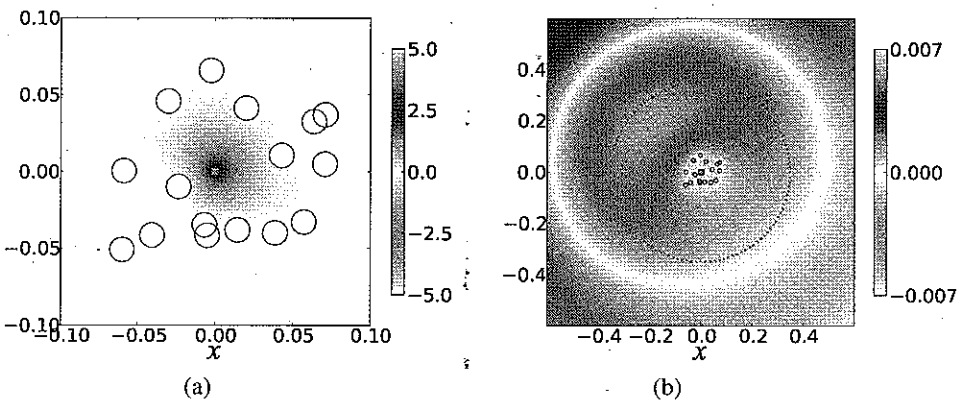

Fig. 8. (a) Snapshot of standing mode pattern radiated by antenna in a cluster of metal particles. (b) Stage 2 reconstructed field.

6. Conclusion

We have modeled the problem of sub-diffraction limited focusing by small dielectric and metallic scatterers in the optical domain for 2D geometries. Focusing well below the free-space

#119185 - $15.00 USD Received 5 Nov 2009; revised 16 Dec 2009; accepted 28 Dec 2009; published 12 Jan 2010

diffraction limit is indeed possible in the scattering regime, but as the focusing is not greatly stronger than in the equivalent homogenized regime, it is not clear that there is a significant advantage to this approach. However, since in the scattering regime the spot size is determined by a few local scatterers, it may be that with careful design work hot-spot engineering could allow for SDL focusing with a smaller number of scatterers than would be required in the homogenized regime.

Acknowledgments

This work was supported by a merit grant from the national facility of the National Computing Infrastructure. CUDOS is an Australian Research Council Centre of Excellence.

#119185 - $15.00 USD Received 5 Nov 2009; revised 16 Dec 2009; accepted 28 Dec 2009; published 12 Jan 2010